Inorganic Chemistry

Article

pubs.acs.org/IC

Ni^{I}/Ru^{II} Model for the Ni–L State of the [NiFe]Hydrogenases: Synthesis, Spectroscopy, and Reactivity

Geoffrey M. Chambers,[†] Joyee Mitra,[†] Thomas B. Rauchfuss,*[,†] and Matthias Stein*[,‡]

[†]School of Chemical Sciences, University of Illinois, Urbana, Illinois 61801, United States

[‡]Max Planck Institute for Dynamics of Complex Technical Systems, Sandtorstraβe 1, 39106 Magdeburg, Germany

Supporting Information

ABSTRACT: This study describes the characterization of a mixed-valence Ru^{II}/Ni^{I} complex, a structural model for the Ni–L state of the [NiFe]hydrogenases. One-electron oxidation of (cymene)Ru(μ-pdt)Ni(diphos) ($[\mathbf{1}]^0$, diphos = dppe, $C_2H_4(PPh_2)_2$; $[\mathbf{2}]^0$, diphos = dcpe, $C_2H_4(P(C_6H_{11})_2)_2$] affords the mixed-valence cations [(cymene)Ru(pdt)Ni(diphos)]$^+$ ($[\mathbf{1}]^+$ and $[\mathbf{2}]^+$). Crystallographic and spectroscopic measurements indicate that these cations are described as Ru^{II}/Ni^{I}. Although $[\mathbf{1}]^0$ and $[\mathbf{1}]^+$ are very similar structurally, the following changes are notable: the Ni–P distances elongate upon oxidation, and the Ru–Ni distance changes insignificantly. The molecular and electronic structures of the Ni center in $[\mathbf{1}]^+$ approaches that observed in the [NiFe]hydrogenases. Density functional theory calculations indicate that $[\mathbf{1}]^0$ is best described as Ru^{II}/Ni^{0}, consistent with its oxidation to Ru^{II}/Ni^{I} in $[\mathbf{1}]^+$. The fast electron self-exchange rate of 10^7 M^{-1} s^{-1} between $[\mathbf{1}]^0$ and $[\mathbf{1}]^+$ suggests minor reorganization, more consistent with a Ni^0/Ni^I oxidation state change than a Ni^I/Ni^{II} couple. In solution, $[\mathbf{1}]^+$ slowly converts to $[H\mathbf{1}]^+$ and $[\mathbf{1}\text{-}H]^+$, with the latter being a complex of the thioaldehyde $SCHCH_2CH_2S$ arising from C–H activation of the pdt backbone. Treatment of $[\mathbf{1}]^+$ with the H-atom abstracting reagent 2,2,6,6-tetramethylpiperidine-1-oxy also gives $[\mathbf{1}\text{-}H]^+$.

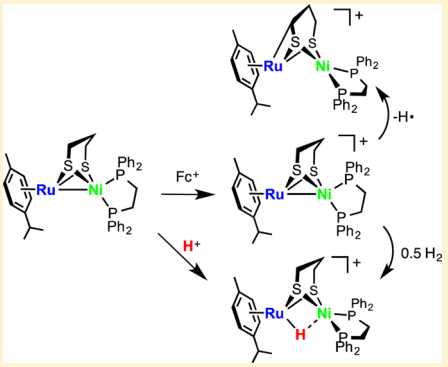

INTRODUCTION

The [NiFe]- and [FeFe]hydrogenases (H_2ases) are bioorganometallic catalysts for two reactions, hydrogen evolution and hydrogen oxidation. These processes proceed via acid–base and redox steps that involve entities that are unusual in organometallic chemistry.[3,4] For example, in the [NiFe]H_2ases, the active site in the catalytic cycle shuttles between diamagnetic Ni^{II}/Fe^{II} and two $S = {}^1/_2$ Ni^{III}/Fe^{II} and Ni^{I}/Fe^{II} states, called Ni–C and Ni–L, respectively (Scheme 1.).[5,6] Ni–A and Ni–B are also $S = {}^1/_2$ Ni^{III}/Fe^{II} states of the oxidized active site but are not part of the catalytic cycle. Spectroscopic studies to date suggest that Ni is the site of all redox processes in the enzyme.[3,6] The three strong-field inorganic ligands (CO and two CN^-) maintain the Fe center in a redox-inactive, low-spin divalent state.

Scheme 1. Formal Relationships between States of Likely Catalytic Roles

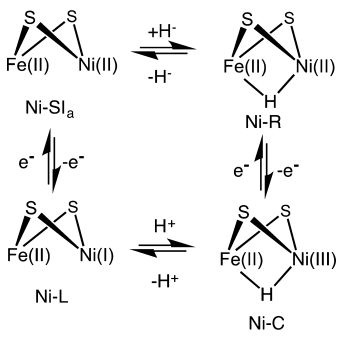

The subject of this report is the Ni–L state, which is proposed to feature a hydride-free Fe^{II}/Ni^{I} active site. Ni–L is generated by photolysis of the Ni–C state at low temperature (T < 100 K). Upon illumination, the electron paramagnetic resonance (EPR) spectrum loses coupling to the bridging hydride,[7,8] consistent with a formal reduction from Ni^{III} to Ni^{I} by transfer of a proton from the Ni–Fe center to a terminal cysteine residue.[9,10] Recent work proposes that Ni–L (sometimes call Ni–R*) is a catalytic intermediate that links Ni–SI_a to Ni–C.[11] Biophysical studies of these enzymes have detected the presence of species assigned to Ni–L even in the absence of photoactivation,[12] suggesting that this state has a catalytic role.

Molecular models of Ni–C, Ni–SI_a, and Ni–L remain elusive, although synthetic analogues for the Ni–R state now exist.[13] Initial attempts to model the Ni–L state started with the Ni^{I}/Fe^{I} complex $(CO)_3Fe(\mu\text{-pdt})Ni(dppe)$[14] and derivatives. One-electron oxidation of this species affords the mixed-valence cation $[(CO)_3Fe(\mu\text{-pdt})Ni(dppe)]^+$.[15,16] Detailed structural and spectroscopic measurements indicate, however, that this species and its substituted derivatives are described as Ni^{II}/Fe^{I},[15,16] *not* the Ni^{I}/Fe^{II} configuration assigned to the Ni–L state (Figure 1). Owing to the pair of CO ligands, the Fe^{I}

Received: February 17, 2014
Published: March 31, 2014

   dx.doi.org/10.1021/ic500389p | Inorg. Chem. 2014, 53, 4243–4249

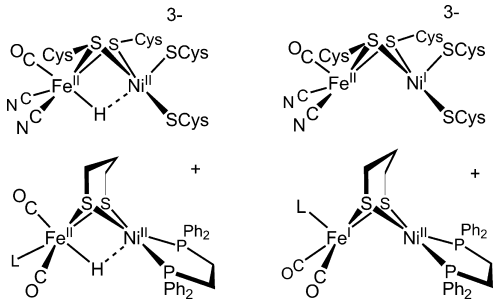

Figure 1. Top: Structures proposed for the active site of the Ni−R and Ni−L states of the [NiFe]hydrogenase (possible protonation states of terminal ScCys ligands not shown).[1] Bottom: Crystallographically established[2] structures of representative Ni−Fe models, with the latter being Fe^{I}/Ni^{II}, not Fe^{II}/Ni^{I}; L = CO, PR_3.

center in these complexes is less prone to oxidation than the nickel(I) diphosphine site. We reasoned that changing from $[(CO)_2LFe(\mu\text{-pdt})Ni(dppe)]^+$ to $[(arene)Ru(\mu\text{-pdt})Ni(dppe)]^+$ would relocalize the singly occupied molecular orbital (SOMO) from Fe/Ru to Ni. As described in this paper, this idea guided the preparation of a Ru^{II}/Ni^{I} complex, structurally and spectroscopically reminiscent of the Ni−L state.

A recent publication from this laboratory describes the starting compounds employed in our quest for a bimetallic complex containing Ni^{I}. Specifically, the reaction of $[(cymene)RuCl_2]_2$ with Ni(pdt)(dppe) affords the Ru^{II}/Ni^{II} species of $[(cymene)Ru(Cl)(pdt)Ni(dppe)]^+$ ($[\mathbf{1}Cl]^+$). Two-electron reduction of this cation gives (cymene)Ru(pdt)Ni(dppe) ($[\mathbf{1}]^0$), which is easily oxidized. This reduced species was tentatively assigned as Ru^{II}/Ni^{0},[17] a two-electron mixed-valence species.[18] The present work confirms this description, verifying that the (arene)ruthenium center in this Ru−Ni complex (and possibly others[19]) is redox-inactive.

RESULTS AND DISCUSSION

The synthetic transformations described in this work are summarized in Scheme 2.

Cyclic voltammetry shows that $[\mathbf{1}]^0$ and its dcpe analogue, $[\mathbf{2}]^0$, undergo reversible one-electron oxidation respectively at −1.0 and −0.8 V versus $Fc^{+/0}$.[17] On a preparative scale, a solution of $[\mathbf{1}]^0$ was treated with 1 equiv of $FcBAr^F_4$ to afford a red-violet solution, from which $[(cymene)Ru(\mu\text{-pdt})Ni(dppe)]BAr^F_4$ ($[\mathbf{1}]BAr^F_4$) could be isolated as a dark-red solid. Similar behavior was observed for the oxidation of $[\mathbf{2}]^0$ to $[(cymene)Ru(\mu\text{-pdt})Ni(dcpe)]BAr^F_4$ ($[\mathbf{2}]BAr^F_4$).

The X-band EPR spectrum of a toluene/PhCl solution of $[\mathbf{1}]BAr^F_4$ is rhombic, with g values of 2.240, 2.053, and 2.025 (Figure 2). To our surprise, the **g** tensor principal values of $[\mathbf{1}]^+$

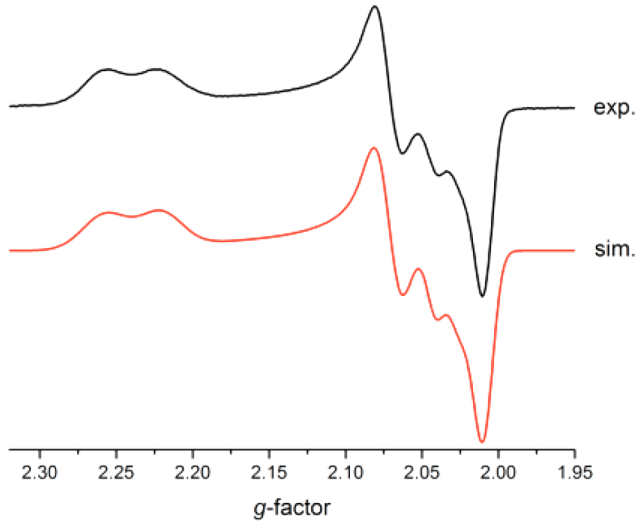

Figure 2. X-band EPR spectrum of a frozen PhCl/PhMe solution (110 K) of $[\mathbf{1}]BAr^F_4$ and the simulated spectrum. Simulation parameters: g_x = 2.025; g_y = 2.053; g_z = 2.240; $A_{x,y,z}(^{31}P)$ = 139.4, 171.2, 147.4 MHz.

are already similar to those from Ni−L of *Thiocapsa roseopersicina*, $g_{x,y,z}$ = 2.29, 2.13, and 2.05.[7] The spectrum of $[\mathbf{1}]^+$ exhibits hyperfine coupling to one $I = {}^1/_2$ center corresponding to 139, 171, and 147 MHz. This coupling is associated with the ^{31}P center and suggests that in $[\mathbf{1}]^+$ at least part of the SOMO extends to the diphosphine ligand. Additionally, it is apparent from the spectrum that the two phosphine centers contribute very differently to the SOMO. The EPR spectrum for $[\mathbf{2}]^+$ is similar to that for $[\mathbf{1}]^+$ with g values of 2.271, 2.066, and 2.027; it exhibits greater superhyperfine coupling, suggesting a slightly different SOMO compared to that of $[\mathbf{1}]^+$ (see the Supporting Information, SI).

Ni^{I} complexes of the type $[Ni(PR_3)_4]^+$ with monodentate ligands typically adopt tetrahedral structures.[20,21] An axial EPR spectrum was reported for $[Ni(dppe)_2]^+$, with g values of 2.134 and 2.030 (g_{iso} = 2.07) and an isotropic phosphorus hyperfine interaction with $a_{iso}(^{31}P)$ = 177 MHz[22] The superhyperfine coupling for Ni^{I} bound to a pair of phosphine thioether ligands is A = 118 and 126 MHz.[23] EPR spectra of Ni^{I} with $g_{\|} > g_{\perp} >$ 2.0 are typical of a ground state with primarily $d_{x^2-y^2}$ character.[24]

Crystallographic analysis revealed that the structures of $[\mathbf{1}]BAr^F_4$ and its precursor **1** are very similar (Figures 3 and 4). The angle between the P_2Ni and S_2Ni planes changes from 84.91° to 71.78° upon oxidation of $[\mathbf{1}]^0$ (Figure 4). Oxidation of the Ni center is indicated by the lengthening of the Ni−P_{avg} distance by 0.089 Å. A similar effect is observed in $[Ni(diphosphine)_2]^{n+}$ complexes, where the Ni−P distances elongate by 0.078 Å upon oxidation from Ni^{0} to Ni^{I},[21] reflecting the diminished role of π-back-bonding in the Ni^{I} state.

Density Functional Theory (DFT) Calculations. Calculations reproduced well the structural features of crystallographic analysis of the reduced complex (Table S3 in the SI). Average deviations of 0.02−0.03 Å in bond lengths and 2−3° in

Scheme 2

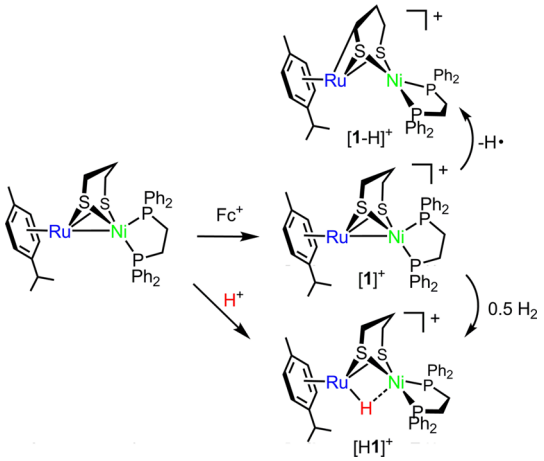

dx.doi.org/10.1021/ic500389p | Inorg. Chem. 2014, 53, 4243−4249

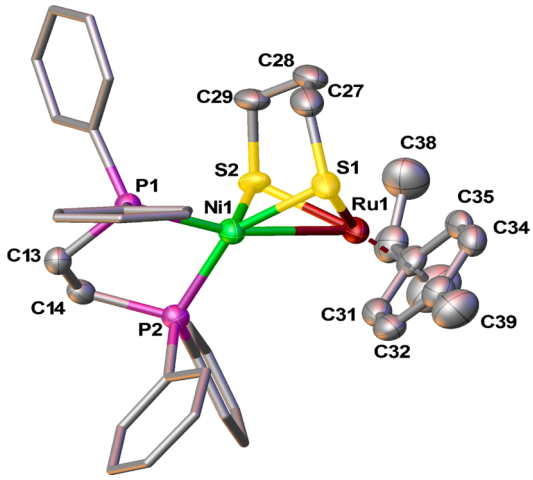

Figure 3. Structure of the non-H atoms of the cation [(cymene)Ru(pdt)Ni(dppe)]$^+$ in [**1**]BAr$^F_4$. Thermal ellipsoids are shown at the 50% level.

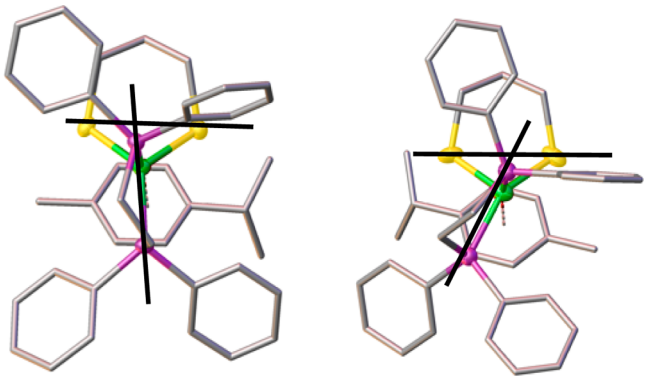

Figure 4. Structures of [**1**]^0 (left) and of [**1**]$^+$ (right) viewed down the Ni–Ru bond axis. Bold lines highlight the dihedral angles for NiP_2 versus NiS_2 planes.

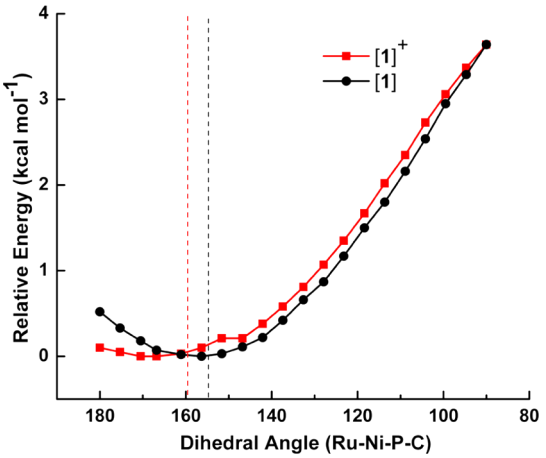

Figure 5. Variation in energy relative to the crystallographically obtained structures for both [**1**]^0 and [**1**]$^+$ obtained from a scan of the Ru–Ni–P–C dihedral angle. The vertical lines indicate the crystallographically obtained dihedral angles.

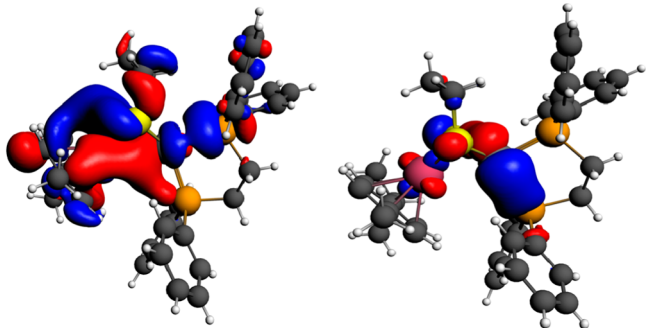

Figure 6. DFT-calculated isocontour plots (isovalue 0.04) of selected molecular orbitals for [**1**]^0. Left: a doubly occupied orbital depicting Ru–Ni interaction (HOMO−2) is delocalized over the entire metal–ligand framework. Right: the HOMO is principally centered on Ni, both S centers, and one of the two P ligand centers.

bond angles were obtained. The structure of the oxidized complex [**1**]$^+$ was also reproduced accurately by DFT calculations (see Table S3 in the SI). Of particular interest is the twist for the NiS_2P_2 site relative to the Ni–Ru vector, which was crystallographically determined to be 70° in [**1**]$^+$. The calculations gave a value of 74°. Such a small difference between single-crystal X-ray diffraction results and gas-phase or solution (COSMO) calculations is not unusual and may originate from crystal-packing effects. A scan of the dihedral angle along the Ru–Ni–P–C vector for both [**1**]^0 and [**1**]$^+$ revealed a shallow potential energy surface at twist angles close to the crystallographically determined values (Figure 5).

Calculations of complex [**1**]^0 were carried out with the aim of assigning the oxidation states of the metal centers. The HOMO of [**1**]^0 is highly localized on Ni (48%), whereas Ru contributes about 13% (see Figure S9 in the SI). Interaction of the two metal sites is manifested in HOMO−2. This orbital is characterized as a Ru–Ni-bonding interaction that is delocalized over the metal centers and ligands (Figure 6). A multipole-derived atomic charge analysis up to a quadrupolar level (MDC-q) was conducted,[25] which is used to assess the charge on the metal centers and surrounding ligand atoms, revealed a positive charge of +0.50 on the Ru and a slight positive charge of +0.05 on the Ni atom in [**1**]^0.

To benchmark the above description of [**1**]^0, the electronic structure of (dppe)Ni(pdt)$Fe(CO)_3$ was reexamined. This Ni–Fe complex is described as a Fe^I/Ni^I complex:[14] MDC analysis revealed that the charges on the Ni and Fe centers are very close (Table S4 in the SI), in contrast to the case for [**1**]^0.

In the calculations, the Ni–P bonds elongate from 2.12 Å in [**1**]^0 to 2.18 Å in [**1**]$^+$, in agreement with the crystallographic results and consistent with a decrease in the P–Ni π-back-bonding upon oxidation. The Ni–S bonds become unsymmetrical (from 2.26 Å each in [**1**]^0 to 2.24 and 2.30 Å in [**1**]$^+$).

The noninnocence and partial covalent character of the Ni–P and Ni–S bonds are revealed by analyzing the redistribution of charges upon oxidation. The MDC-q values at the metal ions are almost unchanged (+0.46 on Ru and −0.03 on Ni) in [**1**]$^+$ compared to those (+0.50 on Ru and +0.05 on Ni) in [**1**]^0. The MDC charges on the P and S ligand atoms, on the other hand, increase upon oxidation.

In the case of [**1**]$^+$, the calculated unpaired spin distribution shows that it extends only to *one* P atom of the dppe ligand (Figure 7). In [**1**]^0, the HOMO mainly consists of Ni $3d_{x^2-y^2}$ (42%) and Ni $3d_{xz}$ (6%). Some structural reorganization and redistribution of the orbital occupancies result from one-electron oxidation. In [**1**]$^+$, the SOMO is made up of 14% of the Ni $3d_{x^2-y^2}$ orbital, 12% of one S 3p orbital, and 11% of the

dx.doi.org/10.1021/ic500389p | *Inorg. Chem.* 2014, 53, 4243−4249

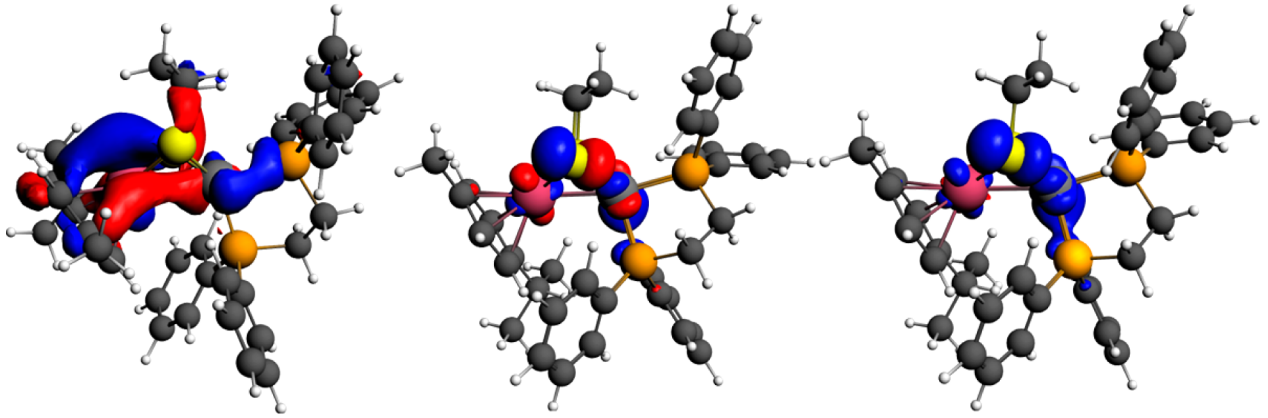

Figure 7. HOMO−1 (left) depicting Ru−Ni interaction, SOMO (middle) from the restricted open-shell calculation, and isocontour plot of the total unpaired spin density distribution at 0.003 e^- (right) from the unrestricted open-shell DFT calculations of complex $[\mathbf{1}]^+$.

Ni $3d_{xy}$ orbital. This occupancy can explain the rhombic EPR spectrum of $[\mathbf{1}]^+$ (see below). The contribution of Ru-based orbitals is almost unchanged from $[\mathbf{1}]^0$ to $[\mathbf{1}]^+$ ($[\mathbf{1}]^0$ HOMO, 5% Ru $4d_{yz}$, 4% Ru $4d_{xz}$, 4% Ru d_{z^2}; $[\mathbf{1}]^+$ HOMO, 6% Ru $4d_{z^2}$, 5% Ru $4d_{xy}$, 2% Ru $4d_{xz}$), showing that Ru is not redox-active in this complex. Indeed, the molecular orbitals with greater Ru character are the lower lying HOMO−1 (34% Ru $4d_{x^2-y^2}$) and HOMO−2 (33% Ru $4d_{yz}$, 12% Ru $4d_{xz}$, 12% Ru $4d_{z^2}$).

The Ni−Ru-bonding interaction in $[\mathbf{1}]^0$ is manifested in the HOMO−2 (Figure 6) and thus is unaffected by oxidation. In $[\mathbf{1}]^+$, a similar Ni−Ru interaction can be found in the HOMO−1 (Figure 7). Oxidation of $[\mathbf{1}]^0$ results in some redistribution of the orbital occupancies of Ni, S, and P and is manifested by elongation of the Ni−S and Ni−P bonds. The Ru center is almost unperturbed, as reflected in the almost identical Ni−Ru distances in $[\mathbf{1}]^0$ and $[\mathbf{1}]^+$ (Table 1).

Table 1. Selected Bond Distances (Å) and Angles (deg) for $[\mathbf{1}]^+$ and $[\mathbf{1}]^0$

parameter	$[\mathbf{1}]^+$	$[\mathbf{1}]^{0}$[17]
Ru−Ni	2.5321(8)	2.5539(5)
Ru−cymene (C_6 centroid)	1.699(6)	1.710(5)
Ru−S	2.329(4), 2.324(4)	2.3326(7), 2.3336(7)
Ni−S	2.245(4), 2.275(4)	2.2442(8), 2.2443(9)
$Ni-P_{apical}$	2.242(2)	2.1465(8)
$Ni-P_{basal}$	2.236(2)	2.1542(9)
P−Ni−P	87.13(6)	90.00(3)
S−Ni−S	91.6(2)	91.29(3)
NiS_2/NiP_2 interplanar angle	71.8(2)	84.91(4)

Analysis and Interpretation of EPR Spectra of [1]$^+$. EPR analysis and calculations suggest that the oxidation of $[\mathbf{1}]^{0/+}$ is almost exclusively Ni-based (see below). According to a MDC-q spin population analysis, the unpaired electronic spin is localized at the Ni center (0.54) and to a lesser extent at the ligand S (0.21) and P atoms (0.09). The remaining ∼15% spin is delocalized, but the Ru atom only carries 0.08 e^-. Calculated MDC-q spin densities can be found in the SI (Table S5).

For $[\mathbf{1}]^+$, DFT calculations (Orca B3LYP/def2-TZVP) gave a rhombic **g** tensor with g_x, g_y, g_z = 2.04, 2.05, 2.20 (ADF B3LYP/TZP g_x, g_y, g_z = 2.04, 2.05, 2.22), which agree nicely with those recorded at X-band g_x, g_y, g_z = 2.03, 2.05, 2.24. Only *one* of the two ^{31}P centers carries significant spin density, reflected by a large hyperfine interaction A_x, A_y, A_z = (+141, +148, +192) MHz, yielding an isotropic hyperfine interaction, A_{iso}, of +160 (B3LYP/def2-TZVP results). These calculated values agree well with the measured isotropic hyperfine interaction of +152 MHz. Also the dipolar hyperfine interaction is in good agreement with the calculated one, $A_{dip,calc}$ = (−19, −12, +31) MHz and $A_{dip,exp}$= (−13, −6, +19) MHz. The hyperfine coupling of the second ^{31}P center was smaller by almost a order of magnitude and is not resolved in the EPR spectrum.

In the [NiFe]H_2ases, the photoreduced Ni−L state corresponds to a potential Ni^I species. The EPR spectrum ($g_{x,y,z}$ = 2.30, 2.12, 2.05)[26] is considered to be indicative of a Ni^I species with a $3d_{x^2-y^2}$ ground state.[1,26] Recently, the bonding in Ni−L was reinterpreted in terms of the symmetry-adapted $3d_{x^2}$ and $3d_{z^2-y^2}$ orbitals[9] in which the $3d_{x^2}$ orbitals of Ni and Fe formed bent σ bonding and antibonding interactions, and the electron spin resides in a Ni-based $3d_{z^2-y^2}$ orbital. Depending on the cluster model, calculations on Ni−L indicate that the majority of unpaired spin resides on the Ni atom, between 0.63 and 0.71, and *one* of the four cysteinyl S atoms (0.17−0.22). A very analogous situation is found for $[\mathbf{1}]^+$ (see Table S5 in the SI).

Self-Exchange. These kinetic experiments were undertaken in order to gain further insight into the structural changes attendant to oxidation of $[\mathbf{1}]^0$. ^1H NMR spectra were recorded for solutions of $[\mathbf{1}]^0$ treated with varying equivalents of $FcBAr^F{}_4$ to generate mixtures of $[\mathbf{1}]^0$ and $[\mathbf{1}]^+$. At room temperature, only one set of signals was observed at chemical shifts corresponding to the average of the signals for $[\mathbf{1}]^0$ and $[\mathbf{1}]^+$, weighted according to their mole fractions (Figure 8). The observation of only one set of signals indicates that electron transfer is fast on the NMR time scale. Analysis of the line widths for the averaged signals allowed us to determine the self-exchange rate, which was $(1.0 \pm 0.1) \times 10^7$ M^{-1} s^{-1} (eq 1; the asterisk is an arbitrary label). Self-exchange for the $Fc^{+/0}$ couple is similar.[27] Such fast self-exchange rates indicate that the redox event causes little structural rearrangement.

$$[\mathbf{1}]^0 + [\mathbf{1}^*]^+ \rightleftharpoons [\mathbf{1}]^+ + [\mathbf{1}^*]^0 \quad (1)$$

Reactions of the Ni^I Complex [1]$^+$: H-Atom Abstraction and Hydrogenation. Over the course of several hours at room temperature, tetrahydrofuran (THF)-d_8 solutions of $[\mathbf{1}]^+$ and H_2 gave the diamagnetic hydride $[\mathbf{H1}]^+$ (eq 2).

dx.doi.org/10.1021/ic500389p | Inorg. Chem. 2014, 53, 4243−4249

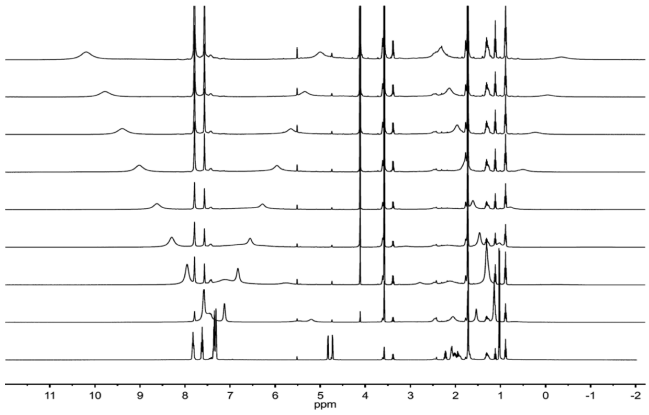

Figure 8. ^{1}H NMR spectra of Ru^{II}/Ni^{0} (bottom) treated with various equivalents of $FcBAr^{F}_{4}$ (ascending). Diamagnetic (unshifted) resonances correspond to $BAr^{F}_{4}{}^{-}$, ferrocene, THF, *n*-pentane, and Et_2O.

$$2[\mathbf{1}]^{+} + H_2 \rightarrow 2[H\mathbf{1}]^{+} \quad (2)$$

Yields are quantitative. Because $[H\mathbf{1}]^{+}$ can be deprotonated, $[\mathbf{1}]^{+}$ is a formal catalyst for oxidation of H_2, although we anticipate that it would be slow-acting.

Analysis of freshly prepared samples of the mixed-valence complex $[\mathbf{1}]BAr^{F}_{4}$ by high-resolution electrospary ionization mass spectrometry (ESI-MS) consistently yielded a dominant ion at one mass unit less than expected (m/z_{obs} = 797.0679 and m/z_{calc} = 798.0756). This difference indicates loss of a H radical to give a new compound, $[\mathbf{1}\text{-H}]^{+}$. Solutions of the red-violet mixed-valence complex $[\mathbf{1}]BAr^{F}_{4}$ were found to be unstable over the course of several days, affording green-brown solutions. ^{1}H and ^{31}P NMR spectroscopic analysis revealed that two predominant complexes are produced, the hydride $[H\mathbf{1}]^{+}$ and the new complex $[\mathbf{1}\text{-H}]^{+}$ (eq 3).

$$2[\mathbf{1}]^{+} \rightarrow [\mathbf{1}\text{-H}]^{+} + [H\mathbf{1}]^{+} \quad (3)$$

Crystallographic analysis showed that $[\mathbf{1}\text{-H}]^{+}$ is a Ru−Ni complex of the ligand $SCHCH_2CH_2S^{x-}$, formally a thiolato-thioaldehyde derived by partial dehydrogenation of propanedithiolate. Complexes of this entity are known[28] and have been generated by radical reactions.[29] Treatment of $[\mathbf{1}]BAr^{F}_{4}$ with 2,2,6,6-tetramethylpiperidine-1-oxy (TEMPO), an H-atom abstracting agent, afforded $[(cymene)Ru(\mu\text{-}SCHCH_2CH_2S)Ni(dppe)]BAr^{F}_{4}$ ($[\mathbf{1}\text{-H}]BAr^{F}_{4}$) in good yield.

The product of dehydrogenation was characterized crystallographically (Figure 9). The μ-thioaldehyde group binds in a η^2 manner to Ru. The Ru adopts a pseudooctahedral geometry and the Ni center is square-planar, suggesting that the thioaldehyde ligand be viewed as the trianion $SCHCH_2CH_2S^{3-}$. The room temperature ^{31}P NMR spectrum of $[\mathbf{1}\text{-H}]^{+}$ exhibits only a single resonance, indicating a dynamic exchange process. Upon cooling of the sample, the resonance broadens and develops into a pair of doubles at −70 °C.

CONCLUSIONS

This study describes the first Ni^{I}-containing bimetallic model for the $[NiFe]H_2$ases. The distorted tetrahedral coordination environment of Ni is unique in Ru−Ni complexes, regardless of the oxidation state.[2,30] In the $[NiFe]H_2$ases, the angle between the $Ni(\mu\text{-}SCys)_2$ and $Ni(term\text{-}SCys)_2$ planes is 69.19°. In the Ni^{I}/Ru^{II} model, the SNiS−PNiP planes are poised at 71.78°. Tetradentate dithiolate ligands, which are traditionally

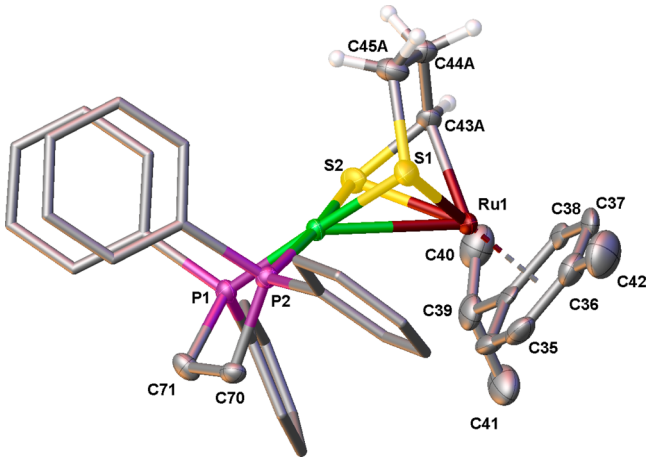

Figure 9. Structure of the cation $[(cymene)Ru(S_2CHCH_2CH_2S)Ni(dppe)]^{+}$ in $[\mathbf{1}\text{-H}]BAr^{F}_{4}$. H atoms, except those in the bridging ligand, have been omitted for clarity. Selected distances (Å) and angles (deg): Ru1−Ni1, 2.7940(5); Ru−centroid, 1.691(3); $Ru-C_{avg}$, 2.203(7); Ru−C43A, 2.143(6); $Ru-S_{avg}$, 2.388(1); S1−Ru−S2, 82.4(1); $Ni-S_{avg}$, 2.1909(9); S1−Ni−S2, 91.94(4); $Ni-P_{avg}$, 2.1653(9); P1−Ni−P2, 84.76(3); S1−C45A, 1.897(5); S2−C43A, 1.716(5).

employed in modeling of the $[NiFe]H_2$ases,[31] cannot accommodate Ni in this biomimetic geometry. This deficiency may be relevant to the limited literature on models for the reduced states of the enzyme.

Both theory and experiment suggest that the reduced model $[\mathbf{1}]^{0}$ is best described as Ni^{0}/Ru^{II}. The main experimental evidence for this assignment is the finding that one-electron oxidation of the proposed Ni^{0}/Ru^{II} species does not result in square-planar Ni (Scheme 3) but retains the nearly tetrahedral

Scheme 3

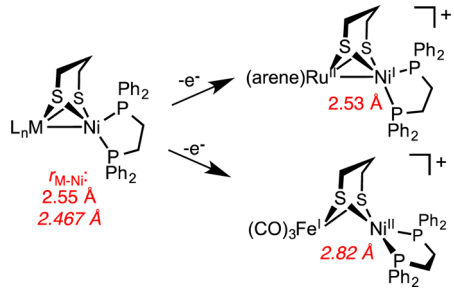

coordination geometry at Ni. Recent work has shown that retention of a close-to-tetrahedral coordination geometry afforded a low-barrier route for heterolytic hydrogen splitting in $[NiFe]H_2$ases.[32] Furthermore, the Ni−P distances elongate upon oxidation, consistent with the $Ni^{0/I}$ couple. The Ni^{0}/Ru^{II} complexes are highly basic: pK_a^{PhCN} = 18.9 for $[H\mathbf{1}]^{+}$ versus 10.7 for $[(CO)_3Fe(\mu\text{-pdt})(\mu\text{-H})Ni(dppe)]^{+}$. The pK_a^{PhCN} increases by 3.6 units upon replacement of dppe by dcpe (to give $[H\mathbf{2}]^{+}$),[17] which also points to Ni as the site of protonation. The final evidence for the Ni^{0}/Ru^{II} and Ni^{I}/Ru^{II} assignments is the high rate of self-exchange, which implies very little structural difference between these states. We anticipate that the self-exchange rates for $[(CO)_{3-x}L_xFe(pdt)Ni(dppe)]^{+/0}$ will prove to be slow because of the accompanying structural rearrangement.[15]

The redox changes of the Ni/Ru complexes are Ni-localized, and it is the initial site of protonation. These findings are

dx.doi.org/10.1021/ic500389p | Inorg. Chem. 2014, 53, 4243−4249

consistent with the oxidation state assignments of Ru^{II}/Ni^{0}. It is tempting therefore to conclude that the Ru center is merely a spectator. Clearly, however, Ru is intimately involved because it binds the hydride ligand more strongly, as evidenced by the metal−hydride distances 1.5404(4) Å (Ru−H) and 1.6542(6) Å (Ni−H).[17] Furthermore, the reduced Ru/Ni complexes are far more basic than the mononuclear Ni complexes. For example, the pK_a^{MeCN} of $[HNi(dppe)_2]^+$ is 14.2,[33] which is 4.7 units lower than that for $[H\mathbf{1}]^+$ (but about 2 units higher than that for $[(CO)_3FeH(pdt)Ni(dppe)]^+$). This enhanced basicity reflects the stabilizing influence of the bimetallic pocket and the high hydricity of Ru^{II}.[33] As proposed by Nicolet et al.,[34] the Ni center in the reduced [NiFe]H_2ases may function as the initial site of protonation prior to conveying the hydride to the redox-inactive d^6 center.

EXPERIMENTAL SECTION

Unless otherwise noted, reactions and manipulations were performed using standard Schlenk techniques at room temperature. Solvents were high-performance liquid chromatography grade and were dried by filtration through activated alumina or distilled under nitrogen over an appropriate drying agent. The reagents were commercially available or have been described in previous publications. ESI-MS data for compounds were acquired using a Waters Micromass Quattro II spectrometer. ^{1}H NMR spectra (500 MHz) were referenced to residual solvent relative to tetramethylsilane. $^{31}P\{^1H\}$ NMR spectra (202 MHz) were referenced to an external 85% H_3PO_4 standard. EPR spectra of mixed-valence complexes were recorded on 1−5 mM solutions in PhCl. The instrument was a Varian E-line 12″ Century Series X-band continuous-wave spectrometer. Spectra were simulated using the program *SIMPOW6*.[24] Fourier transform infrared spectra were recorded on a Perkin-Elmer 100 spectrometer. Crystallographic data were collected using a Siemens SMART diffractometer equipped with a Mo Kα source (λ = 0.71073 Å) and an Apex II detector.

[(cymene)Ru(μ-pdt)Ni(dppe)]BAr^F_4 ([1]BAr^F_4). A solution of $FcBAr^F_4$ (0.0142 g, 0.0135 mmol) in THF (0.5 mL) was added dropwise to a stirred solution of $[\mathbf{1}]^0$ (0.0108 g, 0.0135 mmol) in THF (0.5 mL). The resultant solution gradually became dark red-violet. The product precipitated upon the slow addition of 3 mL of pentane. A dark-red solid was collected by filtration and washed several times with pentane until the filtrate was colorless. Yield: 0.022 g (98%). Anal. Calcd for $C_{71}H_{56}BF_{24}NiP_2RuS_2$ (found): C, 51.31 (50.96); H, 3.40 (3.19). Single crystals were grown by slow diffusion of pentane into a concentrated THF solution. The rate constant for self-exchange for the $[\mathbf{1}]^{0/+}$ couple was determined by ^{1}H NMR spectroscopy for CD_2Cl_2 solutions of $[\mathbf{1}]^0$ treated with varying equivalents of $[Fc]BAr^F_4$.[35] Details are provided in the SI.

[(cymene)Ru(μ-pdt)Ni(dcpe)]BAr^F_4 ([2]BAr^F_4). This compound was generated in solution for EPR characterization in a manner similar to that for $[\mathbf{1}]BAr^F_4$.

Conversion of [1]$^+$ to [H1]$^+$. The hydride $[H\mathbf{1}]BAr^F_4$ was prepared in good yield by stirring a CD_2Cl_2 solution of $[\mathbf{1}]BAr^F_4$ under an atmosphere of H_2 for 12 h. NMR data of the resulting $[H\mathbf{1}]^+$ matched published values.[17]

[(cymene)Ru(μ-SCHCH$_2$CH$_2$S)Ni(dppe)]BAr^F_4 ([1-H]BAr^F_4). A solution of TEMPO (0.0026 g, 0.0166 mmol) in THF (1.0 mL) was added to a solution of $[\mathbf{1}]BAr^F_4$ (0.0302 g, 0.0168 mmol) in THF (1 mL). The solution was stirred for 24 h, during which time the solution became dark green. The solvent was removed under reduced pressure to yield a green residue, which was extracted into THF and recrystallized by vapor diffusion of pentane. The solids were collected by filtration and washed with pentane. Yield: 0.024 g (80%). $^{31}P\{^1H\}$ NMR (THF): δ 61.7. Anal. Calcd for $C_{71}H_{55}BF_{24}NiP_2RuS_2$ (found): C, 51.35 (51.98); H, 3.34 (3.57).

Computational Details. Structural optimizations were performed with *ADF2013*[36] and *Orca 2.9.1*.[37] Both the BP86 exchange-correlation functional[38] and the B3LYP hybrid exchange correlation[39] functional were used for structural optimizations. The resolution-of-identity approximation[40] with a def2-TZVP Ahlrichs basis set[41] was used in *Orca*. The Grimme correction was applied to account for dispersive van der Waals interactions.[42] In ADF calculations, a Slater-type TZP basis set[43] was employed. The scalar-relativistic ZORA Hamiltonian was used during geometry optimization.[44] EPR g values were calculated in the self-consistent spin−orbit-coupled ZORA Hamiltonian in the collinear approximation in ADF and **A** tensors according to ref 45. In *Orca*, calculations of **g** tensors were performed using an effective mean-field spin−orbit coupling operator, with the center of mass as the origin of the **g** tensor.[46] Hyperfine coupling constants were calculated according to Neese.[47]

ASSOCIATED CONTENT

Supporting Information

^{1}H and ^{31}P NMR and IR spectra for new compounds, additional details on the DFT calculations, and CIF files giving X-ray crystallographic data. This material is available free of charge via the Internet at http://pubs.acs.org.

AUTHOR INFORMATION

Corresponding Authors

*E-mail: rauchfuz@illinois.edu.

*E-mail: matthias.stein@mpi-magdeburg.mpg.de.

Notes

The authors declare no competing financial interest.

ACKNOWLEDGMENTS

This research was sponsored by Department of Energy and the Max Planck Society for the Advancement of Science. The authors also acknowledge the support of the International Institute for Carbon Neutral Energy Research (WPI-I^{2}CNER), sponsored by the Japanese Ministry of Education, Culture, Sports, Science and Technology. MS is grateful to the Research Center Dynamic Systems: Biosystems Engineering funded by the Federal State of Saxony-Anhalt. We thank Danielle Gray for collecting the crystallographic data and advice.

REFERENCES

(1) Stein, M.; van Lenthe, E.; Baerends, E. J.; Lubitz, W. *J. Am. Chem. Soc.* **2001**, *123*, 5839.

(2) Ogo, S.; Kabe, R.; Uehara, K.; Kure, B.; Nishimura, T.; Menon, S. C.; Harada, R.; Fukuzumi, S.; Higuchi, Y.; Ohhara, T.; Tamada, T.; Kuroki, R. *Science* **2007**, *316*, 585. Reynolds, M. A.; Rauchfuss, T. B.; Wilson, S. R. *Organometallics* **2003**, *22*, 1619. Oudart, Y.; Artero, V.; Pécaut, J.; Lebrun, C.; Fontecave, M. *Eur. J. Inorg. Chem.* **2007**, *2007*, 2613.

(3) Ogata, H.; Lubitz, W.; Higuchi, Y. *Dalton Trans.* **2009**, 7577.

(4) Fontecilla-Camps, J. C.; Amara, P.; Cavazza, C.; Nicolet, Y.; Volbeda, A. *Nature* **2009**, *460*, 814.

(5) Vignais, P. M.; Billoud, B. *Chem. Rev.* **2007**, *107*, 4206. Fontecilla-Camps, J. C.; Volbeda, A.; Cavazza, C.; Nicolet, Y. *Chem. Rev.* **2007**, *107*, 4273.

(6) Lubitz, W.; Reijerse, E.; van Gastel, M. *Chem. Rev.* **2007**, *107*, 4331.

(7) Whitehead, J. P.; Gurbiel, R. J.; Bagyinka, C.; Hoffman, B. M.; Maroney, M. J. *J. Am. Chem. Soc.* **1993**, *115*, 5629.

(8) Brecht, M.; van Gastel, M.; Buhrke, T.; Friedrich, B.; Lubitz, W. *J. Am. Chem. Soc.* **2003**, *125*, 13075.

(9) Kampa, M.; Pandelia, M.-E.; Lubitz, W.; van Gastel, M.; Neese, F. *J. Am. Chem. Soc.* **2013**, *135*, 3915.

(10) Lubitz, W.; Brecht, M.; Foerster, S.; Stein, M.; Higuchi, Y.; Buhrke, T.; Friedrich, B. *EPR in the 21st Century*; Elsevier: New York, 2002; p 437.

(11) Lill, S. O. N.; Siegbahn, P. E. M. *Biochemistry* **2009**, *48*, 1056.

(12) Roessler, M. M.; Evans, R. M.; Davies, R. A.; Harmer, J.; Armstrong, F. A. *J. Am. Chem. Soc.* **2012**, *134*, 15581.

(13) Barton, B. E.; Rauchfuss, T. B. *J. Am. Chem. Soc.* **2010**, *132*, 14877. Ogo, S.; Ichikawa, K.; Kishima, T.; Matsumoto, T.; Nakai, H.; Kusaka, K.; Ohhara, T. *Science* **2013**, *339*, 682.
(14) Zhu, W.; Marr, A. C.; Wang, Q.; Neese, F.; Spencer, D. J. E.; Blake, A. J.; Cooke, P. A.; Wilson, C.; Schröder, M. *Proc. Natl. Acad. Sci. U. S. A.* **2005**, *102*, 18280.
(15) Schilter, D.; Nilges, M. J.; Chakrabarti, M.; Lindahl, P. A.; Rauchfuss, T. B.; Stein, M. *Inorg. Chem.* **2012**, *51*, 2338−2348.
(16) Schilter, D.; Rauchfuss, T. B.; Stein, M. *Inorg. Chem.* **2012**, *51*, 8931.
(17) Chambers, G. M.; Angamuthu, R.; Gray, D. L.; Rauchfuss, T. B. *Organometallics* **2013**, *32*, 6324.
(18) Rosenthal, J.; Bachman, J.; Dempsey, J. L.; Esswein, A. J.; Gray, T. G.; Hodgkiss, J. M.; Manke, D. R.; Luckett, T. D.; Pistorio, B. J.; Veige, A. S.; Nocera, D. G. *Coord. Chem. Rev.* **2005**, *249*, 1316.
(19) Ogo, S. *Chem. Commun.* **2009**, 3317.
(20) Gleizes, A.; Dartiguenave, M.; Dartiguenave, Y.; Galy, J.; Klein, H. F. *J. Am. Chem. Soc.* **1977**, *99*, 5187.
(21) Wiedner, E. S.; Yang, J. Y.; Chen, S.; Raugei, S.; Dougherty, W. G.; Kassel, W. S.; Helm, M. L.; Bullock, R. M.; Rakowski DuBois, M.; DuBois, D. L. *Organometallics* **2011**, *31*, 144.
(22) Bowmaker, G. A.; Boyd, P. D. W.; Campbell, G. K.; Hope, J. M.; Martin, R. L. *Inorg. Chem.* **1982**, *21*, 1152.
(23) Kim, J. S.; Reibenspies, J. H.; Darensbourg, M. Y. *J. Am. Chem. Soc.* **1996**, *118*, 4115.
(24) Nilges, M. J.; Matteson, K.; Belford, R. L. In *ESR Spectroscopy in Membrane Biophysics, Biological Magnetic Resonance*; Hemminga, M. A., Berliner, L., Eds.; Springer: New York, 2007.
(25) Swart, M.; van Duijnen, P. T.; Snijders, J. G. *J. Comput. Chem.* **2001**, *22*, 79.
(26) Foerster, S.; Stein, M.; Brecht, M.; Ogata, H.; Higuchi, Y.; Lubitz, W. *J. Am. Chem. Soc.* **2003**, *125*, 83.
(27) McManis, G. E.; Nielson, R. M.; Gochev, A.; Weaver, M. J. *J. Am. Chem. Soc.* **1989**, *111*, 5533.
(28) Seyferth, D.; Womack, G. B.; Song, L. C.; Cowie, M.; Hames, B. W. *Organometallics* **1983**, *2*, 928. Huang, Y.; Etkin, N.; Heyn, R. R.; Nadasdi, T. T.; Stephan, D. W. *Organometallics* **1996**, *15*, 2320.
(29) Schenk, W. A. *Dalton Trans.* **2011**, *40*, 1209.
(30) Oudart, Y.; Artero, V.; Pécaut, J.; Fontecave, M. *Inorg. Chem.* **2006**, *45*, 4334. Oudart, Y.; Artero, V.; Norel, L.; Train, C.; Pécaut, J.; Fontecave, M. *J. Organomet. Chem.* **2009**, *694*, 2866. Canaguier, S.; Fourmond, V.; Perotto, C. U.; Fize, J.; Pécaut, J.; Fontecave, M.; Field, M. J.; Artero, V. *Chem. Commun.* **2013**, *49*, 5004. Matsumoto, T.; Kure, B.; Ogo, S. *Chem. Lett.* **2008**, *37*, 970. Matsumoto, T.; Kabe, R.; Nonaka, K.; Ando, T.; Yoon, K.-S.; Nakai, H.; Ogo, S. *Inorg. Chem.* **2011**, *50*, 8902. Zheng, C.; Kim, K.; Matsumoto, T.; Ogo, S. *Dalton Trans.* **2010**, *39*, 2218. Kim, K.; Matsumoto, T.; Robertson, A.; Nakai, H.; Ogo, S. *Chem.—Asian J.* **2012**, *7*, 1394.
(31) Ohki, Y.; Tatsumi, K. *Eur. J. Inorg. Chem.* **2011**, *2011*, 973.
(32) Bruschi, M.; Tiberti, M.; Guerra, A.; De Gioia, L. *J. Am. Chem. Soc.* **2014**, *136*, 1803.
(33) Tilset, M. In *Comprehensive Organometallic Chemistry III*; Crabtree, R. H., Mingos, D. M. P., Eds.; Elsevier: Oxford, U.K., 2007; p 279.
(34) Nicolet, Y.; de Lacey, A. L.; Vernede, X.; Fernandez, V. M.; Hatchikian, E. C.; Fontecilla-Camps, J. C. *J. Am. Chem. Soc.* **2001**, *123*, 1596.
(35) Jameson, D. L.; Anand, R. *J. Chem. Educ.* **2000**, *77*, 88.
(36) ADF2013, SCM, Theoretical Chemistry, Vrije Universiteit: Amsterdam, The Netherlands, http://www.scm.com. te Velde, G.; Bickelhaupt, F. M.; Baerends, E. J.; Guerra, C. F.; Van Gisbergen, S. J. A.; Snijders, J. G.; Ziegler, T. *J. Comput. Chem.* **2001**, *22*, 931.
(37) Neese, F. *WIREs Comput. Mol. Sci.* **2012**, *2*, 73.
(38) Becke, A. D. *Phys. Rev. A* **1988**, *38*, 3098. Perdew, J. P. *Phys. Rev. B* **1986**, *33*, 8822. Perdew, J. P. *Phys. Rev.* **1986**, *34*, 7406.
(39) Becke, A. D. *J. Chem. Phys.* **1993**, *98*, 5648. Lee, C.; Yang, W.; Parr, R. G. *Phys. Rev. B* **1988**, *37*, 785. Stephens, P. J.; Devlin, F. J.; Chabalowski, C. F.; Frisch, M. J. *J. Phys. Chem.* **1994**, *98*, 11623. Vosko, S. H.; Wilk, L.; Nusair, M. *Can. J. Phys.* **1980**, *58*, 1200.
(40) Neese, F. *J. Comput. Chem.* **2003**, *24*, 1740.
(41) Schaefer, A.; Huber, C.; Ahlrichs, R. *J. Chem. Phys.* **1994**, *100*, 5829. Weigend, F.; Ahlrichs, R. *Phys. Chem. Chem. Phys.* **2005**, *7*, 3297.
(42) Grimme, S. *J. Comput. Chem.* **2006**, *27*, 1787.
(43) van Lenthe, E.; Baerends, E. J. *J. Comput. Chem.* **2003**, *24*, 1142.
(44) van Lenthe, E.; Baerends, E. J.; Snijders, J. G. *J. Chem. Phys.* **1993**, *99*, 4597.
(45) van Lenthe, E.; van der Avoird, A.; Wormer, P. E. S. *J. Chem. Phys.* **1998**, *108*, 4783. van Lenthe, E.; Baerends, E. J. *J. Chem. Phys.* **2000**, *112*, 8279. van Lenthe, E.; Wormer, P. E. S.; van der Avoird, A. *J. Chem. Phys.* **1997**, *107*, 2488.
(46) Neese, F. *J. Chem. Phys.* **2005**, *122*, 034107. Neese, F. *J. Chem. Phys.* **2001**, *115*, 11080.
(47) Neese, F. *J. Phys. Chem.* **2003**, *118*, 3939.